pubs.acs.org/Biomac

Article

Facile Synthesis of Poly(ethylene oxide)-Based Self-Healable Dynamic Triblock Copolymer Hydrogels

Youngjoo Hong,[‖] Jung-Min Kim,[‖] Hyunjoon Jung, Kyungtae Park, Jinkee Hong, Soo-Hyung Choi,* and Byeong-Su Kim*

Cite This: https://dx.doi.org/10.1021/acs.biomac.0c01140

Read Online

ACCESS | Metrics & More | Article Recommendations | Supporting Information

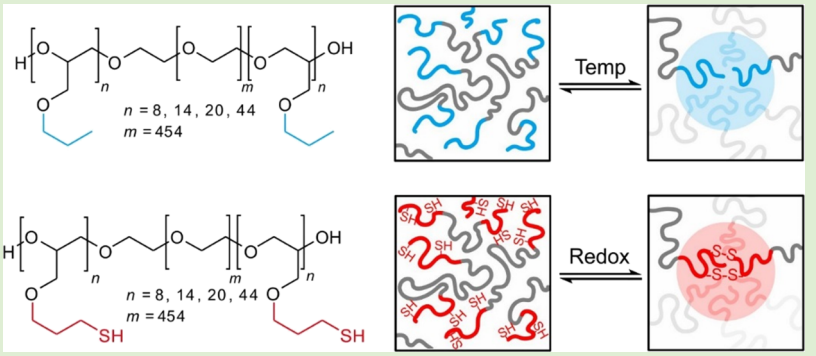

ABSTRACT: Stimuli-responsive smart hydrogels have garnered considerable interest for their potential in biomedical applications. While widely utilized, little is known about the rheological and mechanical properties of the hydrogels with respect to the type of cross-linker in a systematic manner. In this study, we present a facile synthetic route toward ABA triblock copolymer hydrogels based on poly(ethylene oxide) (PEO). Two classes of hydrogels were prepared by employing the functional allyl glycidyl ether (AGE) monomer during the polymerization followed by the subsequent post-polymerization modification of prepared PAGE-*b*-PEO-*b*-PAGE via respective hydrogenation or thiol-ene reaction: (1) chemically cross-linked hydrogels responsive to redox stimuli and (2) physically cross-linked hydrogels responsive to temperature. A series of dynamic mechanical analyses revealed the relaxation dynamics of the associative A block. Most interestingly, the redox-responsive hydrogels demonstrated a highly tunable nature by introducing reducing and oxidizing agents, which provided the self-healing property and injectability. Together with superior biocompatibility, these smart hydrogels offer the prospect of advancing biomedical applications.

INTRODUCTION

A hydrogel comprises a three-dimensional percolated network resulting from hydrophilic polymer chains being held together by various cross-links. Recently, smart hydrogels that are responsive to external stimuli are receiving significant attention because of their biological and biomedical applications, such as drug delivery,[1] cell encapsulation,[2] tissue engineering,[3−5] wound dressing, and contact lenses.[6] They are typically classified into two categories, physical and chemical, based on the type of interaction and cross-linker; for example, physical hydrogels are defined as networks held together primarily by reversible non-covalent interactions including electrostatic,[7] $\pi-\pi$ stacking,[8] hydrophobic,[9−11] and host−guest interactions.[12] On the other hand, chemical hydrogels are formed via reversible yet covalent bonds, such as Diels−Alder chemistry,[13,14] disulfide bonds,[15,16] acylhydrazone bonds,[13,17] and imine bonds.[18]

As a representative system, ABA triblock copolymer hydrogels have been extensively investigated because of well-defined structures with wide ranges of dimensions, mechanical robustness, and versatility.[19−21] When ABA triblock copolymers are dispersed in an aqueous medium, micellar cores are formed by the phase-separated A blocks that are bridged by the hydrophilic B block (typically, poly(ethylene oxide) (PEO)). Thus, the responsive nature of hydrogels is mainly governed by the chemical or physical properties of the A blocks, suggesting that their novel design and synthesis play a significant role in the synthesis of hydrogels.

PEO-based hydrogels are particularly desirable for biomedical applications owing to their non-toxicity, low immunogenicity, and thus excellent biocompatibility. In synthetic approaches toward PEO-based polyethers, A blocks

Received: July 30, 2020
Revised: September 17, 2020

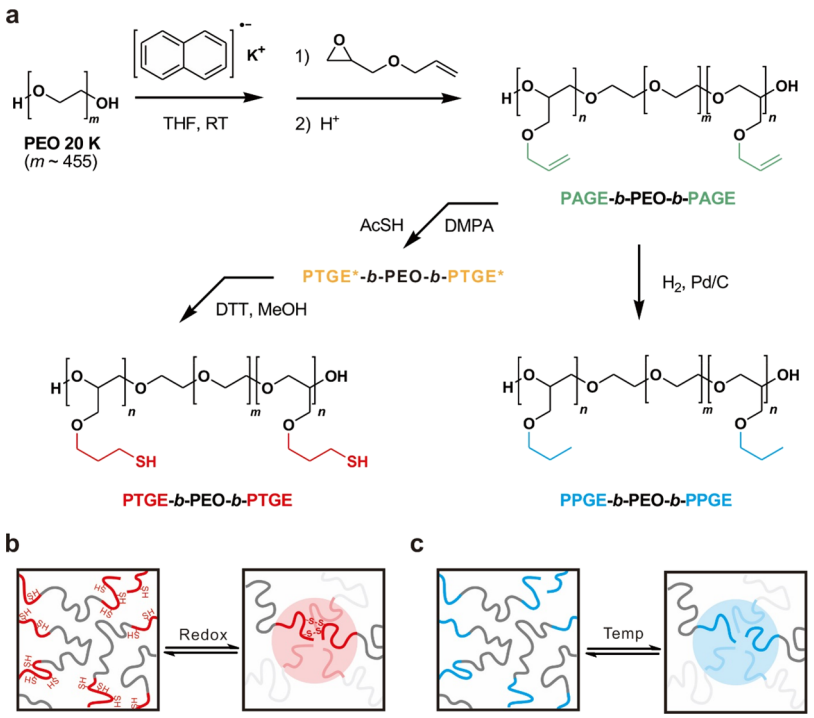

Figure 1. (a) Synthesis of functionalized poly(ethylene oxide) (PEO)-based ABA triblock copolymers with different pendant groups. Schematic representation of the reversible gelation process (b) by the redox reaction between thiol and disulfide groups and (c) according to temperature using hydrophobic interactions. See Experimental Section for details.

can be readily prepared by employing diverse functional monomers[22−31] or post-polymerization modifications.[32−34] In this context, the abundance of available epoxide monomers can provide a wide range of functionality that can be further modified to achieve the desired physical and chemical properties for targeted applications.[24,27,29,35] Alternatively, post-polymerization modification can be an ideal strategy for evaluating various functional groups across a single polymer with an identical degree of polymerization and molecular weight distribution.[28,36−38] Moreover, post-polymerization modification provides the synthesis of polymers with pendant groups through bypassing the limitations of direct polymerization. In view of these benefits, the post-polymerization modification is receiving significant interest to produce well-defined polymers with tailorable properties.

In this study, we present PEO-based ABA triblock copolymer hydrogels in which we integrated both a novel functional monomer and post-polymerization modification to prepare the A blocks, thereby resulting in two classes of hydrogels with the same parent polymer: (1) chemically cross-linked hydrogels responsive to redox stimuli and (2) physically cross-linked hydrogels responsive to temperature. While widely utilized, the rheological and mechanical properties of hydrogels with respect to the type of cross-linker have not yet been uncovered in a systematic manner. Specifically, allyl glycidyl ether (AGE) is presented as a functional monomer to prepare triblock copolymers of PAGE$_n$-*b*-PEO-*b*-PAGE$_n$ via anionic ring-opening polymerization. Subsequent post-polymerization modification of allyl pendant groups on the resulting polymers via hydrogenation or thiol-ene reaction afforded a respective hydrogenated propyl or thiol group in the A block, which provided dynamic hydrogels responsive to either temperature or redox reactions in aqueous media (Figure 1). A comprehensive understanding of their viscoelastic properties was investigated according to the cross-linker type. Moreover, the self-healing of the redox-responsive hydrogel through the redox chemistry of the disulfide-thiol groups along with its excellent biocompatibility was characterized.

EXPERIMENTAL SECTION

Materials. All reagents and solvents were purchased from Sigma-Aldrich (USA), Alfa Aesar (USA), or Tokyo Chemical Industry (Japan) and used as received unless otherwise stated. Tetrahydrofuran (THF) was dried using a solvent purification system (Vacuum Atmospheres, USA) and used immediately. The deuterated NMR solvent chloroform ($CDCl_3$) was purchased from Cambridge Isotope Laboratories (USA). AGE was degassed through several freeze−pump−thaw cycles followed by purification with butyl magnesium chloride by cryo-distillation.

Characterization. ^{1}H NMR spectra were recorded on an Agilent 400 MHz spectrometer at room temperature using $CDCl_3$ as a solvent. Gel permeation chromatography (GPC; Agilent 1200 series, Agilent Technologies, USA) measurements were performed with dimethylformamide (DMF) as an eluent at 30 °C at a flow rate of 1.0 mL min^{-1} using a refractive index (RI) detector with poly(ethylene glycol) (PEG) as a standard (M_p = 500−2,700,000; Sigma-Aldrich). Fourier-transform infrared (FT-IR) spectra were recorded on an Agilent Cary 630 FT-IR spectrometer equipped with an attenuated total reflection (ATR) module. Differential scanning calorimetry (DSC) was carried out with a temperature increment of 10 °C min^{-1} under N_2 (DSC25, TA Instruments, USA).

Synthesis of PAGE-*b*-PEO-*b*-PAGE. PAGE-*b*-PEO-*b*-PAGE polymers were synthesized via anionic ring-opening polymerization of AGE using α,ω-hydroxy-terminated PEO (M_n = 20 kDa) as a macroinitiator, as described elsewhere.[39] The syntheses of the precursor ABA triblock copolymers ($\mathbf{P_8}$, $\mathbf{P_{14}}$, $\mathbf{P_{20}}$, and $\mathbf{P_{44}}$) were carried out in a 500 mL Schlenk flask under an inert argon atmosphere. The reactor was flame dried under vacuum and refilled with argon three times. As a representative example, for the synthesis of ABA triblock copolymer $\mathbf{P_8}$, PEO (20 g, 1.0 mmol) was placed in a flask under nitrogen flow and dried overnight under high vacuum.

https://dx.doi.org/10.1021/acs.biomac.0c01140
Biomacromolecules XXXX, XXX, XXX−XXX

Anhydrous THF was added, and the mixture was stirred at 40 °C. Potassium naphthalenide (0.30 M in THF) was added dropwise via a syringe until a light green color persisted in the solution, indicating the complete deprotonation of the PEO macroinitiator. Next, AGE (3.6 g, 32 mmol) was added and polymerized at 40 °C for 24 h. The reaction was quenched with methanol (MeOH), and the $\mathbf{P}_8$ copolymer was precipitated from hexane. M_n and dispersity (Đ, M_w/M_n) were determined via ^{1}H NMR and GPC analyses, respectively. ^{1}H NMR ($\mathbf{P}_8$) (400 MHz, $CDCl_3$): δ 5.98−5.83 (m, 1H), 5.31−5.21 (d, 1H), 5.21−5.12 (d, 1H), 4.03−3.96 (d, 1H), 3.70−3.38 (m, 96H). GPC ($\mathbf{P}_8$) (DMF, PEG standard): M_n = 20,000 and $Đ$ = 1.04.

General Procedure for Hydrogenation. The precursor polymer ($\mathbf{P}_8$) (5 g, 0.23 mmol) and Pd/C (0.5 g, 10 wt % of the polymer) were dissolved in 10 mL of MeOH in a reaction tube. The reaction mixture was degassed via three freeze−pump−thaw cycles and then stirred under a hydrogen atmosphere at room temperature. After 6 h, the reaction mixture was filtered through a Celite and 0.45 μm PTFE membrane filter. The resulting polymers (H series polymers) were obtained as a powder and dried under high vacuum for 1 day, giving an isolated yield of typically 80−90%. ^{1}H NMR ($\mathbf{H}_8$) (400 MHz, $CDCl_3$): δ 3.70−3.38 (m, 94H), 1.65−1.54 (m, 2H), 0.97−0.89 (t, 3H). GPC ($\mathbf{H}_8$) (DMF, PEG standard): M_n = 17,000 and $Đ$ = 1.06.

General Procedure for the Thiol-Ene Reaction and Reduction. This procedure is based upon the modification of a previous method.[40] The thiol-ene reaction between the $\mathbf{P}_8$ polymer (5 g, 0.23 mmol) and thioacetic acid (0.84 g, 11.04 mmol; 3.0 equiv for each "ene" moiety) was carried out using 2,2-dimethoxy-2-phenyl-acetophenone (DMPA; 47 mg, 0.184 mmol; 0.05 equiv for each "ene" moiety) as a photoinitiator in 70 mL of methanol. The reaction mixture was degassed via nitrogen bubbling and irradiated with UV light (λ = 365 nm) for 2 h until complete disappearance of the alkene peaks, as indicated by ^{1}H NMR analysis. Subsequently, MeOH was removed under reduced pressure, the concentrated mixture was precipitated twice into cold ether, and the resulting polymer was dried under high vacuum for 1 day, affording the thioacetate-modified polymer $\mathbf{S}'$, giving an isolated yield of typically 80−90%. ^{1}H NMR ($\mathbf{S}'_8$) (400 MHz, $CDCl_3$): δ 3.70−3.38 (m, 82H), 2.95 (t, J = 6.9 Hz, 2H), 1.88 (s, 3H), 1.02−0.93 (m, 2H). GPC ($\mathbf{S}'_8$) (DMF, PEG standard): M_n = 21,100 and $Đ$ = 1.12.

The $\mathbf{S}'_8$ polymer (4 g, 0.17 mmol) was dissolved in a mixture of MeOH and H_2O (50 mL, 1/1 v/v), after which NaOH (0.44 mg, 11.12 mmol; 4.0 equiv for each "thioester" moiety) was added to proceed with the hydrolysis, during which the reaction was heated at 70 °C for 24 h. The mixture was cooled to room temperature, and the pH was adjusted to 8.5 with 1 M HCl solution and further reduced with dithiothreitol (DTT) (0.86 g, 5.56 mmol; 2 equiv for each thiol moiety) for 12 h at room temperature. The obtained polymer $\mathbf{S}_8$ was dialyzed against MeOH and then water (MWCO 12 K dialysis membrane, Fisher Scientific, USA) for 2 days, after which the purified polymer was lyophilized and stored at room temperature as a dry powder.

Preparation of the Hydrogels. For the thermo-responsive hydrogels, H series polymers were dissolved in phosphate-buffered saline (PBS) (pH 7.0) and allowed to equilibrate at 5 °C for at least 12 h. For the redox-responsive hydrogels, S series polymers were dissolved in PBS (pH 7.0) with a predetermined equivalent of DTT followed by equilibration for at least 96 h at room temperature.

Rheology Study. Dynamic mechanical measurements were conducted on an MCR302 rheometer (Anton Paar, Austria) using a parallel plate geometry of 25 mm diameter. Temperature was controlled by using a Peltier accessory, and water evaporation was minimized by utilizing a home-made cover. Hydrogels were loaded between two plates with a gap of approximately 1 mm. Time sweep measurements were performed for 20 min prior to each sequence to confirm the thermal equilibrate state. The temperature dependence between G' and G'' was measured at a frequency of 1 Hz and a ramping rate of 2 °C/min. Frequency sweep measurements were performed from 0.1 to 100 rad/s at 0.5 and 1% strain amplitudes for the **H** and the **S** hydrogels, respectively, at which the linear viscoelastic regimes were confirmed at 25 °C. Cyclic shear strain experiments were performed at strains of 1 to 300% with an interval of 3 min per cycle at a frequency of 1 Hz.

Self-Healing Test. Two hydrogel plates were made in the 3 cm × 2 cm PTFE container. Then, 3 wt % of the $\mathbf{S}_8$ polymer was dissolved in PBS (pH 7.0) with 3 equiv of DTT followed by equilibration for 96 h at room temperature. The preparation of the colored hydrogel proceeded analogously except that rhodamine B was added with PBS. Each hydrogel plate was cut in half, and then the colored hydrogel (with rhodamine B) and the colorless hydrogel (without rhodamine B) were placed side by side in the sealed container. To compare the self-healing property under redox condition, one hydrogel plate was applied with a solution of H_2O_2, which equals to 3 equiv of DTT, at the cutting edge and surface, while the other hydrogel plate was left without H_2O_2 treatment. After equilibrating for 24 h, self-healing was evaluated based on whether contact surfaces of the hydrogel were split or merged when external force was applied.

Injectability Test. Here, 3 wt % of the $\mathbf{S}_8$ polymer was dissolved in DI water with rhodamine B and 2 equiv of DTT in the 10 mL vial followed by equilibration for 96 h at room temperature. The $\mathbf{S}_8$ hydrogel was filled in a 3 mL syringe with an 18G needle for the injectability test. To compare the injectable property with the $\mathbf{H}_{14}$ hydrogel, the $\mathbf{H}_{14}$ hydrogel was prepared by dissolving 3 wt % of the $\mathbf{H}_8$ polymer in DI water with methylene blue followed by equilibration for 24 h in a refrigerator at 4 °C and then 24 h at room temperature.

Cytotoxicity Assay. The viability of human dermal fibroblasts (HDF, Lonza, Switzerland) and green fluorescence protein-labeled human umbilical vein endothelial cells (GFP-HVC, Angio Proteomie, USA) was used to test the biocompatibility of the hydrogels. HDFs and GFP-HVCs were cultured by following the protocol from the cell supplier in the dark at 37 °C and 5% CO_2. For the cell growth media, we used Dulbecco's modified Eagle's medium (DMEM; Gibco Life Technologies, USA) with 10% fetal bovine serum (FBS, Welgene, Korea) and 1% penicillin/streptomycin (Gibco Life Technologies) for the HDFs and EGM-2 (Lonza) with 1% penicillin/streptomycin (Gibco Life Technologies) for the GFP-HVCs. We seeded 1.0×10^4 cells with 1 mL of the medium in each well of a 24-well plate. Before treating the cells with the hydrogels, we prepared the $\mathbf{H}_{14}$ and $\mathbf{S}_8$ hydrogels as 3 wt % in each vial via cooling for 1 h in a refrigerator at 4 °C followed by gelation at room temperature for 2 days. After 24 h of incubation, the hydrogel was treated using a Transwell permeable support (CLS3413, Corning Incorporated, USA). We loaded 150 μL of the hydrogel in the hanging insert and then put it into each well. After 24 h of treatment, the hanging well inserts were removed and washed with 1× PBS (Gibco Life Technologies), then 800 μL of the growth medium and 80 μL of the cell counting kit-8 reagent (CCK-8, D-Plus CCK cell viability assay kit, Dongin LS, Korea) were added followed by incubation for 1.5 h. The medium was collected, and the absorbance at a wavelength of 450 nm was measured using a plate reader (SpectraMax 340 PC, Molecular Devices, San Jose, USA) for 24 and 72 h.

Statistical Analyses. Two-sample t-tests were conducted to evaluate the statistical reliability of the cell viability assay. The difference between the mean values of the control and sample groups was calculated to assess statistical significance. The symbols * (P-value <0.05), ** (P-value <0.01), and *** (P-value <0.001) are used to indicate the level of significance.

RESULTS AND DISCUSSION

Synthesis of the Triblock Copolymers. The polymerization proceeded via anionic ring-opening polymerization of AGE monomers using PEO (M_n = 20 k) as a macroinitiator initiated by potassium naphthalenide at 40 °C for 24 h (Figure 1). A series of PAGE-*b*-PEO-*b*-PAGE triblock copolymers (denoted as **P** polymers, hereafter) with various molecular weights of the PAGE segments ranging from 1800 to 10,000 g mol^{-1} were successfully prepared by controlling the monomer-

https://dx.doi.org/10.1021/acs.biomac.0c01140
Biomacromolecules XXXX, XXX, XXX−XXX

Table 1. Characterization Data for the Polymers Synthesized in this Study

entry	polymer code	polymer composition	$M_{n,NMR}$[a] (g mol^{-1})	$M_{n,GPC}$[b] (g mol^{-1})	Đ[b]
1	$\mathbf{P}_8$	$PAGE_8$-*b*-PEO-*b*-$PAGE_8$	21,800	20,000	1.04
2	$\mathbf{H}_8$	$PPGE_8$-*b*-PEO-*b*-$PPGE_8$	21,820	17,000	1.06
3	$\mathbf{S'}_8$[c]	$PTGE_8$-*b*-PEO-*b*-$PTGE_8$	23,030	21,100	1.12
4	$\mathbf{P}_{14}$	$PAGE_{14}$-*b*-PEO-*b*-$PAGE_{14}$	21,670	20,500	1.05
5	$\mathbf{H}_{14}$	$PPGE_{14}$-*b*-PEO-*b*-$PPGE_{14}$	21,700	18,200	1.05
6	$\mathbf{S'}_{14}$[c]	$PTGE_{14}$-*b*-PEO-*b*-$PTGE_{14}$	23,830	22,500	1.19
7	$\mathbf{P}_{20}$	$PAGE_{20}$-*b*-PEO-*b*-$PAGE_{20}$	24,600	21,600	1.04
8	$\mathbf{H}_{20}$	$PPGE_{20}$-*b*-PEO-*b*-$PPGE_{20}$	24,640	19,000	1.05
9	$\mathbf{S'}_{20}$[c]	$PTGE_{20}$-*b*-PEO-*b*-$PTGE_{20}$	27,680	25,000	1.07
10	$\mathbf{P}_{44}$	$PAGE_{44}$-*b*-PEO-*b*-$PAGE_{44}$	30,000	24,400	1.03

[a]Determined via ^{1}H NMR spectroscopy in $CDCl_3$. [b]Measured using GPC in DMF using the RI signal and PEG standard. [c]Thioester form before deprotection.

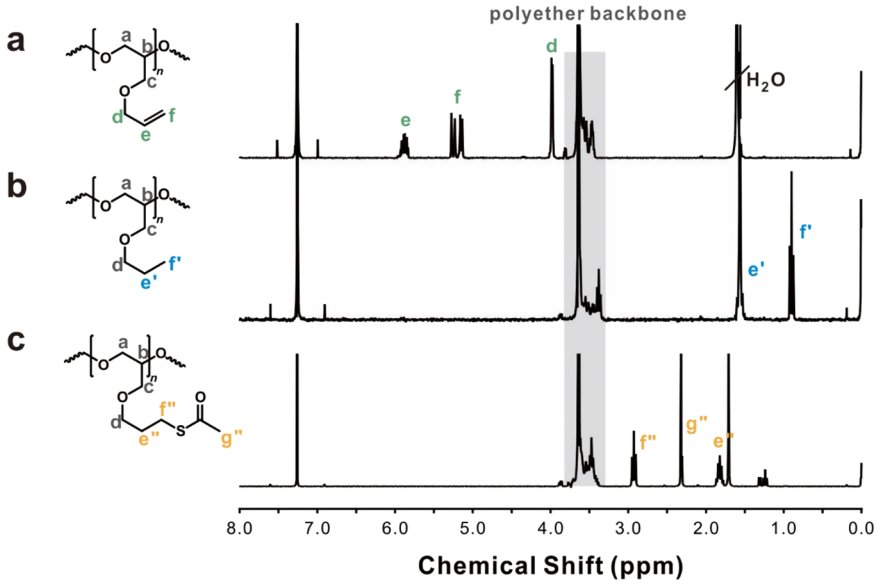

Figure 2. Post-polymerization modification of (a) precursor $\mathbf{P}_{14}$ triblock copolymers (entry 4 in Table 1) via (b) hydrogenation or (c) thiol-ene reaction with the corresponding ^{1}H NMR spectra of the resulting **P**, **H**, and **S′** polymers (entries 4–6 in Table 1, respectively).

to-initiator ratio (Table 1). The obtained precursor **P** triblock copolymers containing reactive allyl groups in the end blocks were characterized via ^{1}H NMR and GPC (Figures S1 and S2 in the Supporting Information). The ^{1}H NMR spectra of the **P** polymers clearly show the characteristic peaks corresponding to the allyl protons (3.99, 5.18, 5.28, and 5.91 ppm) and the polyether backbone (3.24–4.05 ppm). Based on the ^{1}H NMR results, the number-average molecular weight ($M_{n,NMR}$) was calculated by using the peak integral ratio between the PEO backbone and the allyl protons in the PAGE block. Furthermore, the GPC results of the triblock copolymers show a monomodal distribution with narrow dispersity (Đ = 1.03–1.09) using the PEO standard in DMF, which clearly shifted to a higher-molecular-weight region with increasing molecular weight (Table 1 and Figures S1 and S2).

It is known that isomerization of the allyl group occurs during polymerization at a high temperature.[39] In this study, it was determined that except for $\mathbf{P}_8$, the degree of isomerization of the allyl group was below 15% owing to the relatively low polymerization temperature of 40 °C (Figure S3). The molecular weight and dispersity of the polymers were not affected by the extent of the isomerization. While the isomerization did not affect the hydrogenation reaction afterward, the thiol-ene reaction with the corresponding thiol groups could have been affected by the isomerization.

Post-Polymerization Modifications. After the successful polymerization of $PAGE_n$-*b*-PEO-*b*-$PAGE_n$ (**P**) polymers, we performed post-polymerization modification of the pendant allyl moieties via hydrogenation or the thiol-ene reaction. At first, hydrogenation was carried out with H_2 in the presence of a Pd/C catalyst to afford the $PPGE_8$-*b*-PEO-*b*-$PPGE_8$ (**H**) polymers (Figure 1). The ^{1}H NMR spectrum clearly confirmed the complete conversion of the pendant allyl groups by the disappearance of the allylic peaks after hydrogenation (Figure 2b). Furthermore, the GPC analysis of the **H** polymers showed a monomodal distribution without a noticeable change in dispersity (Figure S4).

In parallel, using the precursor **P** polymers, we performed photochemical-mediated thiol-ene addition of the pendant allyl moieties with thioacetic acid to provide the $PTGE_{20}$-*b*-PEO-*b*-$PTGE_{20}$ polymers (Figure 1).[36,38] Photoinitiator DMPA and 3 equiv of thioacetic acid were used for complete conversion while suppressing the undesirable side reaction. ^{1}H NMR spectroscopy confirmed the conversion of the pendant allyl groups with the concomitant appearance of thioester peaks (Figure 2c). The GPC analysis of the **S′** polymers showed peak shift according to conversion of allyl to the thioester group

https://dx.doi.org/10.1021/acs.biomac.0c01140
Biomacromolecules XXXX, XXX, XXX–XXX

(Figure S5). It is of note that while we observed the presence of the intermolecularly cross-linked polymers, the fraction is relatively small and, more importantly, this cross-link would not contribute to redox-responsive behavior. In addition, FT-IR spectra revealed a new band at 1691 cm^{-1} corresponding to the thioester group (Figure S6).

DSC studies provided the glass-transition temperature (T_g) and melting temperature (T_m) of a series of **P**, **H**, and **S′** polymers (Table S1 and Figure S7). T_m was constant throughout the samples prepared due to the highly crystalline nature of the PEO block in the ABA triblock copolymers. This phenomenon was similarly observed in the case of the hydrogenated **H** polymers and **S′** polymers. In summary, the melting point and glass-transition temperature of the polymers were changed by the type of A block.

Once all of the polymers had been synthesized, hydrolysis of the thioester in the **S′** polymers was performed using excess NaOH followed by reduction using DTT (Figure 1). Interestingly, the **S** polymers spontaneously formed a hydrogel upon reduction to the thiol during the dialysis for purification. This observation indicates the spontaneous formation of intermolecular disulfide bonds to drive the hydrogel formation from free thiol-containing **S** polymers. While other characterizations such as ^{1}H NMR and GPC could not access the structure of the **S** polymers, the FT-IR spectra clearly confirmed the successful reduction by the disappearance of the thioester peak at 1691 cm^{-1} with the appearance of the disulfide bond peak at 560 cm^{-1} (Figure S6). Furthermore, characteristic Raman peaks at 509, 517, and 640 cm^{-1} for the **S** polymers were attributed to the formation of disulfide bonds (Figure S8).

Thermo-responsive Hydrogels. Initially, the PPGE$_n$-*b*-PEO-*b*-PPGE$_n$ (**H** series) triblock copolymers exhibited the formation of hydrogels when dissolved in an aqueous medium (Figure S9). It was also observed that the degree of polymerization influenced the formation of the hydrogels. Among the **H** series polymers, the temperature-responsive properties of the $\mathbf{H_8}$ and $\mathbf{H_{14}}$ hydrogels were examined by dynamic mechanical measurements. As shown in Figure 3, temperature-dependent rheological properties were monitored in terms of storage modulus (G') and loss modulus (G'') for the 3 wt % $\mathbf{H_8}$ and $\mathbf{H_{14}}$ hydrogels. G' was lower than G″ at a low temperature, whereas G' became dominant over G″ at a high temperature, indicating the thermo-responsive sol−gel transition of the hydrogels. As the temperature increased, the end blocks of the PPGE became hydrophobic and segregated into micellar domains that are bridged by PEO blocks, resulting in well-defined hydrogels.[41,42] Previously, the lower critical solution temperature (LCST) behavior of poly(alkyl glycidyl ether) has been observed.[43−45] As a representative example, Aoki et al. pioneered to present the LCST behavior of glycidyl ether derivatives such as methyl, ethyl, and butyl groups in water, in which the transition temperature decreases with the increasing alkyl group.[43] Accordingly, it is expected that the critical temperature for PPGE is lower than 0 °C.

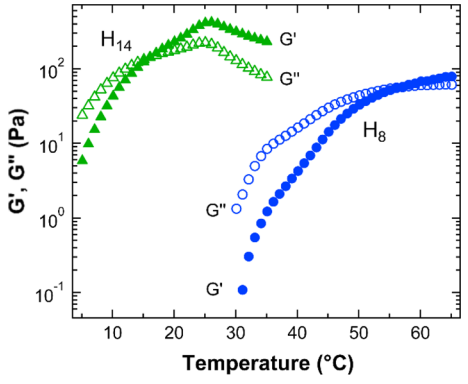

Figure 3. Temperature-dependent storage modulus (G'; closed symbol) and loss modulus (G''; open symbol) for 3 wt % $\mathbf{H_8}$ (circle) and $\mathbf{H_{14}}$ (triangle) hydrogels. The sol−gel transition temperature (T_{gel}) was determined from where G' and G'' intersect.

The sol−gel transition temperatures (T_{gel}) are where G' and G'' meet on a plot of G' and G'' versus temperature, which are 57 and 16 °C for the $\mathbf{H_8}$ and $\mathbf{H_{14}}$ hydrogels, respectively (Figure 3). It is of note that the $\mathbf{H_{20}}$ polymers remained in the gel state within the experimental temperature range, which is mainly attributed to the presence of long hydrophobic end blocks. Thus, T_{gel} is dependent on the end-block length at a fixed polymer concentration, which is in good agreement with previous results.[41,46] Ogura et al. observed that the transition temperature of poly(ethyl glycidyl ether) in water is nearly independent of the molecular weight but highly sensitive to the polymer concentration.[44] The transition temperature decreased by approximately 10 °C as the polymer concentration increased by 1 wt %, which infers that the latter is potentially responsible for the reduced T_{gel} for the longer end-block hydrogel.

Redox-Responsive Hydrogels. Since thiol groups are oxidized to form a disulfide bond reversibly together with the thiol-disulfide exchange chemistry, the end blocks of triblock **S** copolymers can associate to form percolated networks that drive the formation of chemically cross-linked hydrogels (Figure 1).[47,48] In this study, the redox reaction between free thiol and disulfide groups was controlled by the addition of common reducing and oxidizing agents such as DTT and hydrogen peroxide (H_2O_2), respectively.

Figure 4a displays the 3 wt % $\mathbf{S_8}$ hydrogels with various amounts of added DTT and their fluidity upon vial inversion. As the equivalence of DTT increases, more disulfide bonds are reduced to form thiol groups, resulting in gel-to-sol transition of the $\mathbf{S_8}$ hydrogels. It is noteworthy that the disulfide bonds are spontaneously formed during the preparation of polymers, which limits the accurate determination of the number of disulfide bonds in the **S** polymers. Instead, we treated the hydrogel with varying equivalence of DTT on the basis of the thiol groups present in the initial **S** polymers. Moreover, it is important to highlight that the **S** hydrogels were not responsive to temperature within the temperature range measured (Figure S11).

Based on the molecular architecture, the end blocks are segregated to form self-assembled domains mainly due to the disulfide bonds, and those are bridged by PEO midblocks. Since the $\mathbf{H_8}$ polymers are liquid-like in aqueous solution at room temperature, the hydrophobicity of the end blocks can be ruled out. Small-angle X-ray scattering (SAXS) measurements show a structure peak near q = 0.0236 $Å^{-1}$ for 3 wt % $\mathbf{S_8}$ hydrogels with 2 equiv of DTT, which corresponds to the distance between the aggregated domains as approximately 270 Å (Figure S12). The structure peak is still shown for the hydrogels with 9 equiv of DTT, indicating that the self-assembled structure is retained within the experimental conditions, and the complete dissolution of the block copolymers requires the higher equivalence of a DTT. It is

https://dx.doi.org/10.1021/acs.biomac.0c01140
Biomacromolecules XXXX, XXX, XXX−XXX

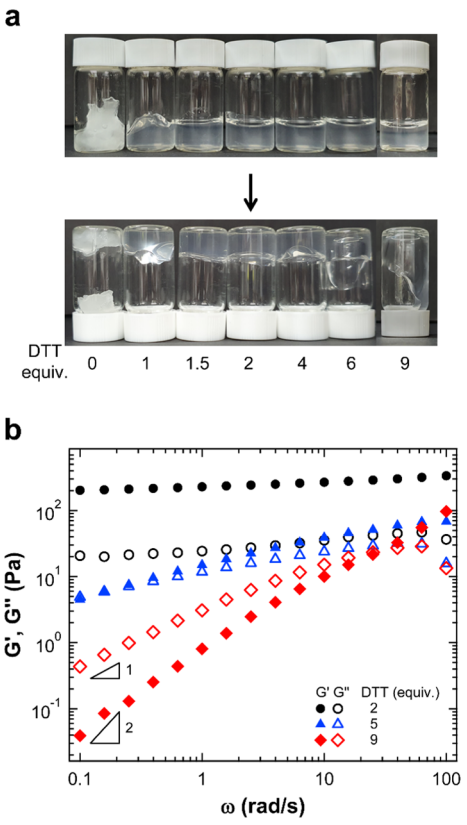

Figure 4. (a) Photographs of 3 wt % $\mathbf{S}_8$ hydrogels with various equivalencies of dithiothreitol (DTT) and the corresponding hydrogels after inversion for 20 s. (b) Frequency-dependent moduli of storage modulus G' (closed symbol) and loss modulus G'' (open symbol) for 3 wt % $\mathbf{S}_8$ hydrogels with respect to the equivalence of DTT. All data collected with various amounts of DTT are presented in Figure S10.

of note that swollen but turbid hydrogels were observed without the addition of DTT as shown in Figure 4a, yet the structure peak was considerably attenuated, which is reasonably attributed to extremely slow chain dynamics. Within the experimental time scale, chain rearrangement to achieve the equilibrium structure was mostly hindered due to the pre-formed disulfide bonds, and thus the bulk structure was retained upon swelling. Since the other **S** hydrogels with longer thiol-containing blocks (i.e., $\mathbf{S}_{14}$ and $\mathbf{S}_{20}$) did not exhibit gel-to-sol transition despite the use of 15 equiv of DTT due to the significantly slow relaxation dynamics of the longer core block lengths (Figure S13),[48,49] we did not investigate the hydrogels obtained from the longer $\mathbf{S}_{14}$ and $\mathbf{S}_{20}$ polymers any further.

The dynamic mechanical measurements show that G' was dominant over G'' and nearly independent of frequency for the 3 wt % $\mathbf{S}_8$ hydrogels with 2 equiv of DTT, which indicates their sturdy gel states (Figure 4b). At a higher amount of DTT, G'' became dominant, and terminal relaxation was observed as $G' \approx \omega^2$ and $G'' \approx \omega^1$, indicating their fluidic sol states. Hydrogel fluidity is primarily dependent on the number of disulfide bonds and the exchange rate of the transition between the disulfide bonds and free thiol groups because the relaxation of an ABA triblock copolymer hydrogel is highly dependent on the single-chain dynamics.[42,49,50] As a representative time scale of the viscoelastic behavior, relaxation time τ is related to the inverse of the frequency where G' and G'' intersect (ω_c) expressed as $\tau = 2\pi/\omega_c$. More disulfide bonds are reduced to free thiol groups at a higher equivalence of DTT, resulting in less hindered chain dynamics and thus shorter τ. As shown in Figure 4b, τ gradually decreases as the amount of DTT in the solution increases.

Owing to the reversible redox reaction, two free thiol groups are oxidized to form a disulfide bond by the addition of an oxidizing agent such as H_2O_2. Figure 5a displays the frequency-dependent moduli of the 3 wt % $\mathbf{S}_8$ hydrogels with varying amounts of H_2O_2 after the formation of hydrogels with the addition of 9 equiv of DTT. Contrary to the reducing agent, the addition of the H_2O_2 oxidant induced more hindered chain dynamics by recovering the disulfide bonds, resulting in the slower hydrogel relaxation. It is noticeable that the τ showed highly reversible responsive behavior toward the dual redox stimuli (Figure 5b), and therefore the relaxation dynamics of the $\mathbf{S}_8$ hydrogels are precisely tunable by three orders of magnitude with the addition of a reducing or oxidizing agent. Furthermore, the frequency-dependent moduli of the hydrogels are highly reversible in response to the equivalence of added reducing or oxidizing agents (Figure S15). We also observed that the hydrogel elasticity, usually estimated via the plateau storage modulus of G', is dependent on the redox environment, which suggests that the hydrogel structure evolves gradually.

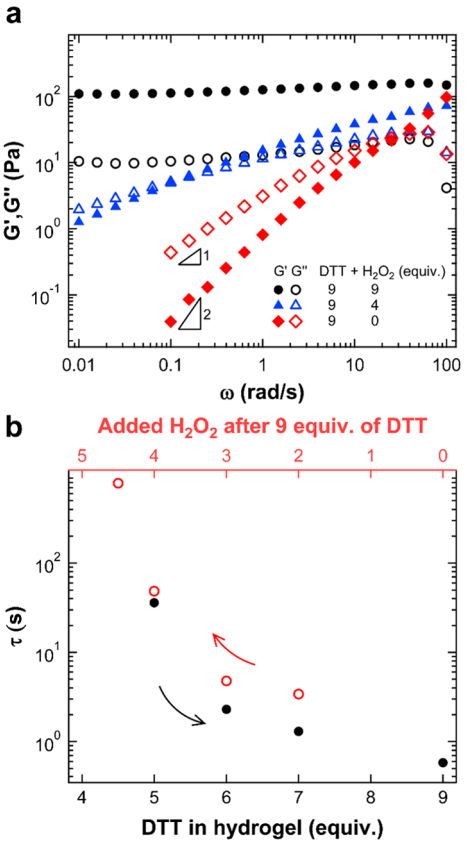

Figure 5. (a) Frequency sweep measurements for the 3 wt % $\mathbf{S}_8$ hydrogel formed with 9 equiv of DTT and varying equiv of H_2O_2. (b) Hydrogel relaxation time (τ) for the 3 wt % $\mathbf{S}_8$ hydrogel as a function of the amount of DTT (black circle) and the amount of H_2O_2 (red circle) after treatment with 9 equiv of DTT. The $\mathbf{S}_8$ hydrogels show highly reversible responsiveness to dual redox stimulation by DTT and H_2O_2. All data collected with various amounts of H_2O_2 are presented in Figure S14.

https://dx.doi.org/10.1021/acs.biomac.0c01140
Biomacromolecules XXXX, XXX, XXX−XXX

Self-Healing Behavior. Based on the highly tunable dynamics of the redox-responsive hydrogels, 3 wt % $\mathbf{S_8}$ hydrogels prepared with 3 equiv of DTT were subjected to a self-healing test (Figure 6). When two pieces of hydrogels, one with the rhodamine B and one without, were placed side by side in a sealed container for 24 h, self-healing of the hydrogel was clearly observed (Figure 6a). However, in clear contrast, when the interface between two pieces was treated with 3 equiv of H_2O_2, the two pieces of hydrogel did not adhere together (Figure 6b). The self-healing property is primarily governed by chain exchange between the segregated domain of the end blocks at the interface being shorter than the hydrogel relaxation time τ.[49,51] Since τ for the $\mathbf{S_8}$ hydrogel without 3 equiv of DTT is much longer than with it, adhesion between the two pieces without cutting lines due to the chain exchange process at the interface requires longer than 24 h. It is also of note that the self-healing property of the $\mathbf{S_8}$ hydrogels is readily controllable by applying the redox agents, and complete recovery can be achieved within the desired time scale. Furthermore, the mechanical properties of the hydrogel after healing can be enhanced by further addition of an oxidizing agent.

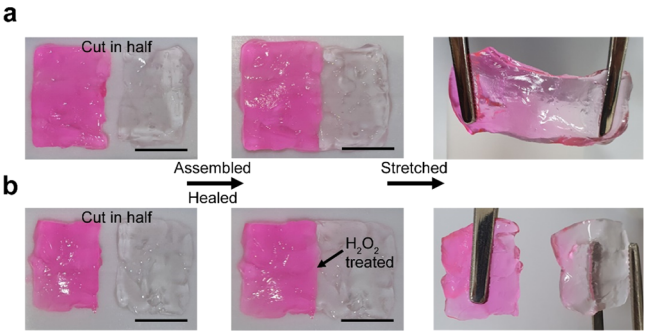

Figure 6. Self-healing testing of the 3 wt % $\mathbf{S_8}$ hydrogels during which two pieces of hydrogel treated with 3 equiv of DTT were placed side by side for 24 h. (a) Self-healing behavior and (b) treatment with H_2O_2 at the interface resulting in the loss of the self-healing property. Rhodamine B was used to aid the visual inspection. The scale bar in the photos is 1 cm. The overall size of the prepared hydrogel was 3 cm × 2 cm.

The shear responsive property of the hydrogels was examined by performing cyclic oscillatory strain jump experiments to provide the potential for injectability by extrusion. Since 3 wt % $\mathbf{S_8}$ hydrogels with 2 equiv of DTT retain the linear viscoelastic regime up to 216% of the applied strain, the cyclic oscillatory strain was abruptly changed from 1 to 300% with an interval of 3 min to induce gel-to-sol transition by shear forces (Figure 7a). The $\mathbf{S_8}$ hydrogel was nearly completely recovered after exposure to the high shear force, indicating that it is potentially applicable to extrusion-based 3D printing. Therefore, we assessed the injectability of the 3 wt % $\mathbf{S_8}$ hydrogel with 2 equiv of DTT using an 18G needle (Figure 7b). We immediately observed gelation after injecting the $\mathbf{S_8}$ hydrogels into the water. Although rhodamine B dye was released by diffusion, the injected hydrogel in deionized water maintained its shape after 1 day. This observation suggests the potential use of hydrogels as a drug delivery reservoir.

In addition, the 3 wt % $\mathbf{H_{14}}$ hydrogels also showed shear-responsiveness and injectability (Figure S16) in good agreement with the previous observations.[21,41,42] Compared to the 3 wt % $\mathbf{S_8}$ hydrogels, the linear viscoelastic regime failed at a less strain of 2% (Figure S11b), and complete recovery after exposure to high shear was not achieved. These results can be attributed to the relatively weak hydrophobic interaction associated with the short core block length of the PPGE blocks.

Cell Viability Assay. Encouraged by the successful synthesis and control over the rheological properties of the prepared hydrogels, we evaluated their biocompatibility to investigate their potential in a biomedical setting. As representative samples, the $\mathbf{S_8}$ and $\mathbf{H_{14}}$ hydrogels were assessed via cell proliferation assays using human dermal fibroblast (HDF) and green fluorescence protein-labeled human umbilical vein endothelial cell (GFP-HVC) as model cell lines. Cell viability in the presence of the respective hydrogels was determined using a Transwell permeable support, which is a well-known biocompatibility assay of hydrogels.[52,53] As shown in Figure 8, both hydrogels showed a steady increase in the viability of each cell line on days 1 and 3 with similar proliferation rates compared to the control. These results demonstrate the excellent biocompatibility of the hydrogels without a noticeable difference compared to the control for

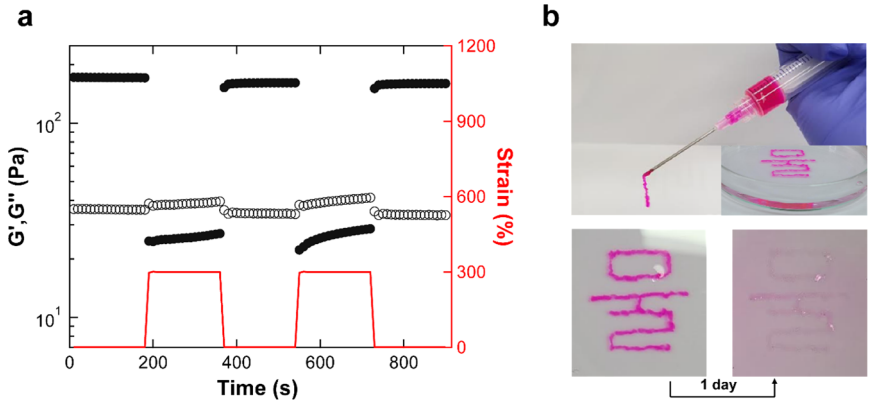

Figure 7. (a) Cyclic oscillatory strain jump experiments for the 3 wt % $\mathbf{S_8}$ hydrogel in the presence of 2 equiv of DTT at a frequency of 1 Hz. Strains of 1 and 300% were applied and repeatedly switched. Solid and open symbols represent storage modulus G′ and loss modulus G″, respectively. (b) (top panel) Photographs of the 3 wt % $\mathbf{S_8}$ hydrogel prepared with 2 equiv of DTT and injected through an 18G needle and (bottom panel) self-sustaining hydrogel in water for more than 1 day showing the release of the rhodamine B dye.

https://dx.doi.org/10.1021/acs.biomac.0c01140
Biomacromolecules XXXX, XXX, XXX−XXX

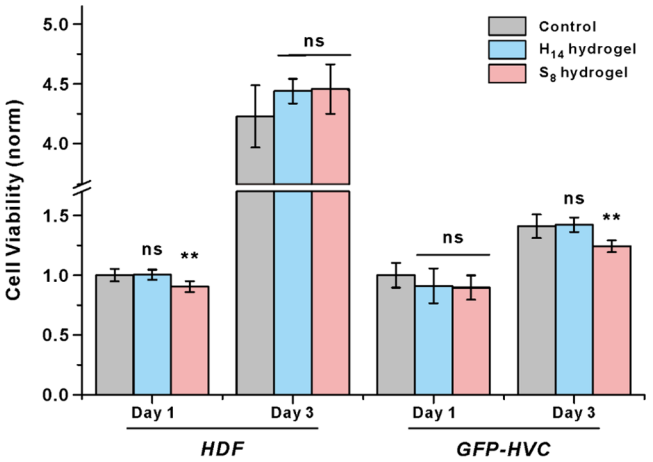

Figure 8. In vitro cell viability assay of the 3 wt % H_{14} and S_8 hydrogels vs. the control via the Transwell permeable support of human dermal fibroblast (HDF) and human umbilical vein endothelial cell (GFP-HVC) cell lines. The averages of five independent experiments are reported as ns (not significant) and ** (*P*-value <0.01) to indicate the level of significance.

both cell lines. Thus, both PEO-based chemical and physical hydrogels can offer new opportunities for biomedical applications.

CONCLUSIONS

In summary, we developed PEO-based ABA triblock copolymer dynamic hydrogels. Employing the anionic ring-opening polymerization of allyl glycidyl ether with subsequent post-polymerization modifications via hydrogenation or thiol-ene reaction afforded the respective hydrogenated propyl group or thiol group in the A block that provided dynamic hydrogels responsive to temperature or redox environment in aqueous media. A comprehensive investigation of the rheological and mechanical properties of the dynamic hydrogels revealed the critical role of the type of cross-linker. The dynamic nature of these hydrogels was further demonstrated via their self-healing property. Together with their excellent cell viability, these dynamic hydrogels based on an all-polyether platform offer a new class of biomaterials with highly tunable chemical and physical properties.

ASSOCIATED CONTENT

Supporting Information

The Supporting Information is available free of charge at https://pubs.acs.org/doi/10.1021/acs.biomac.0c01140.

Additional ^{1}H NMR, GPC, FT-IR, Raman, and DSC data of the polymers; rheology, SAXS, and photographic images of the hydrogels (PDF)

AUTHOR INFORMATION

Corresponding Authors

Soo-Hyung Choi − *Department of Chemical Engineering, Hongik University, Seoul 04066, Republic of Korea;* orcid.org/0000-0002-4078-6285; Email: shchoi@hongik.ac.kr

Byeong-Su Kim − *Department of Chemistry, Yonsei University, Seoul 03722, Republic of Korea;* orcid.org/0000-0002-6419-3054; Email: bskim19@yonsei.ac.kr

Authors

Youngjoo Hong − *Department of Chemistry, Yonsei University, Seoul 03722, Republic of Korea*

Jung-Min Kim − *Department of Chemical Engineering, Hongik University, Seoul 04066, Republic of Korea*

Hyunjoon Jung − *Department of Chemical Engineering, Hongik University, Seoul 04066, Republic of Korea*

Kyungtae Park − *Department of Chemical and Biochemical Engineering, Yonsei University, Seoul 03722, Republic of Korea*

Jinkee Hong − *Department of Chemical and Biochemical Engineering, Yonsei University, Seoul 03722, Republic of Korea;* orcid.org/0000-0003-3243-8536

Complete contact information is available at: https://pubs.acs.org/10.1021/acs.biomac.0c01140

Author Contributions

‖Y.H. and J.-M.K. contributed equally to this work.

Notes

The authors declare no competing financial interest.

ACKNOWLEDGMENTS

This work was supported by Samsung Research Funding & Incubation Center of Samsung Electronics under project number SRFC-MA1602-07.

REFERENCES

(1) Jeong, B.; Bae, Y. H.; Lee, D. S.; Kim, S. W. Biodegradable Block Copolymers as Injectable Drug-Delivery Systems. *Nature* **1997**, *388*, 860−862.

(2) Slaughter, B. V.; Khurshid, S. S.; Fisher, O. Z.; Khademhosseini, A.; Peppas, N. A. Hydrogels in Regenerative Medicine. *Adv. Mater.* **2009**, *21*, 3307−3329.

(3) Drury, J. L.; Mooney, D. J. Hydrogels for Tissue Engineering: Scaffold Design Variables and Applications. *Biomaterials* **2003**, *24*, 4337−4351.

(4) Moutos, F. T.; Freed, L. E.; Guilak, F. A Biomimetic Three-Dimensional Woven Composite Scaffold for Functional Tissue Engineering of Cartilage. *Nat. Mater.* **2007**, *6*, 162−167.

(5) Tang, J. D.; Mura, C.; Lampe, K. J. Stimuli-Responsive, Pentapeptide, Nanofiber Hydrogel for Tissue Engineering. *J. Am. Chem. Soc.* **2019**, *141*, 4886−4899.

(6) Willis, S. L.; Court, J. L.; Redman, R. P.; Wang, J.-H.; Leppard, S. W.; O'Byrne, V. J.; Small, S. A.; Lewis, A. L.; Jones, S. A.; Stratford, P. W. A Novel Phosphorylcholine-Coated Contact Lens for Extended Wear Use. *Biomaterials* **2001**, *22*, 3261−3272.

(7) Alvarez-Lorenzo, C.; Bromberg, L.; Concheiro, A. Light-Sensitive Intelligent Drug Delivery Systems. *Photochem. Photobiol.* **2009**, *85*, 848−860.

(8) Cui, H.; Shao, J.; Wang, Y.; Zhang, P.; Chen, X.; Wei, Y. PLA-PEG-PLA and Its Electroactive Tetraaniline Copolymer as Multi-interactive Injectable Hydrogels for Tissue Engineering. *Biomacromolecules* **2013**, *14*, 1904−1912.

(9) Miquelard-Garnier, G.; Demoures, S.; Creton, C.; Hourdet, D. Synthesis and Rheological Behavior of New Hydrophobically Modified Hydrogels with Tunable Properties. *Macromolecules* **2006**, *39*, 8128−8139.

(10) Mihajlovic, M.; Staropoli, M.; Appavou, M.-S.; Wyss, H. M.; Pyckhout-Hintzen, W.; Sijbesma, R. P. Tough Supramolecular Hydrogel Based on Strong Hydrophobic Interactions in a Multiblock Segmented Copolymer. *Macromolecules* **2017**, *50*, 3333−3346.

(11) Verkoyen, P.; Dreier, P.; Bros, M.; Hils, C.; Schmalz, H.; Seiffert, S.; Frey, H. "Dumb" pH-Independent and Biocompatible Hydrogels Formed by Copolymers of Long-Chain Alkyl Glycidyl Ethers and Ethylene Oxide. *Biomacromolecules* **2020**, *21*, 3152−3162.

(12) Li, Z.; Zheng, Z.; Su, S.; Yu, L.; Wang, X. Preparation of a High-Strength Hydrogel with Slidable and Tunable Potential Functionalization Sites. *Macromolecules* **2016**, *49*, 373−386.
(13) Yu, F.; Cao, X.; Du, J.; Wang, G.; Chen, X. Multifunctional Hydrogel with Good Structure Integrity, Self-Healing, and Tissue-Adhesive Property Formed by Combining Diels−Alder Click Reaction and Acylhydrazone Bond. *ACS Appl. Mater. Interfaces* **2015**, *7*, 24023−24031.
(14) Koehler, K. C.; Anseth, K. S.; Bowman, C. N. Diels−Alder Mediated Controlled Release from a Poly(ethylene glycol) Based Hydrogel. *Biomacromolecules* **2013**, *14*, 538−547.
(15) Wu, D.-C.; Loh, X. J.; Wu, Y.-L.; Lay, C. L.; Liu, Y. 'Living' Controlled *in Situ* Gelling Systems: Thiol−Disulfide Exchange Method toward Tailor-Made Biodegradable Hydrogels. *J. Am. Chem. Soc.* **2010**, *132*, 15140−15143.
(16) Barcan, G. A.; Zhang, X.; Waymouth, R. M. Structurally Dynamic Hydrogels Derived from 1,2-Dithiolanes. *J. Am. Chem. Soc.* **2015**, *137*, 5650−5653.
(17) Buhler, E.; Sreenivasachary, N.; Candau, S.-J.; Lehn, J.-M. Modulation of the Supramolecular Structure of G-Quartet Assemblies by Dynamic Covalent Decoration. *J. Am. Chem. Soc.* **2007**, *129*, 10058−10059.
(18) Boehnke, N.; Cam, C.; Bat, E.; Segura, T.; Maynard, H. D. Imine Hydrogels with Tunable Degradability for Tissue Engineering. *Biomacromolecules* **2015**, *16*, 2101−2108.
(19) Zhang, G.; Chen, Y.; Deng, Y.; Wang, C. A Triblock Copolymer Design Leads to Robust Hybrid Hydrogels for High-Performance Flexible Supercapacitors. *ACS Appl. Mater. Interfaces* **2017**, *9*, 36301−36310.
(20) Zhang, G.; Chen, Y.; Deng, Y.; Ngai, T.; Wang, C. Dynamic Supramolecular Hydrogels: Regulating Hydrogel Properties through Self-Complementary Quadruple Hydrogen Bonds and Thermo-Switch. *ACS Macro Lett.* **2017**, *6*, 641−646.
(21) Shafranek, R. T.; Leger, J. D.; Zhang, S.; Khalil, M.; Gu, X.; Nelson, A. Sticky Ends in a Self-Assembling ABA Triblock Copolymer: The Role of Ureas in Stimuli-Responsive Hydrogels. *Mol. Syst. Des. Eng.* **2019**, *4*, 91−102.
(22) Verkoyen, P.; Frey, H. Amino-Functional Polyethers: Versatile, Stimuli-Responsive Polymers. *Polym. Chem.* **2020**, *11*, 3940−3950.
(23) Song, J.; Hwang, E.; Lee, Y.; Palanikumar, L.; Choi, S.-H.; Ryu, J.-H.; Kim, B.-S. Tailorable Degradation of pH-Responsive All Polyether Micelles via Copolymerisation with Varying Acetal Groups. *Polym. Chem.* **2019**, *10*, 582−592.
(24) Herzberger, J.; Niederer, K.; Pohlit, H.; Seiwert, J.; Worm, M.; Wurm, F. R.; Frey, H. Polymerization of Ethylene Oxide, Propylene Oxide, and Other Alkylene Oxides: Synthesis, Novel Polymer Architectures, and Bioconjugation. *Chem. Rev.* **2016**, *116*, 2170−2243.
(25) Ahn, G.; Kweon, S.; Yang, C.; Hwang, J. E.; Kim, K.; Kim, B.-S. One-Pot Synthesis of Hyperbranched Polyamines Based on Novel Amino Glycidyl Ether. *J. Polym. Sci., Part A: Polym. Chem.* **2017**, *55*, 4013−4019.
(26) Song, S.; Lee, J.; Kweon, S.; Song, J.; Kim, K.; Kim, B.-S. Hyperbranched Copolymers Based on Glycidol and Amino Glycidyl Ether: Highly Biocompatible Polyamines Sheathed in Polyglycerols. *Biomacromolecules* **2016**, *17*, 3632−3639.
(27) Son, S.; Shin, E.; Kim, B.-S. Redox-Degradable Biocompatible Hyperbranched Polyglycerols: Synthesis, Copolymerization Kinetics, Degradation, and Biocompatibility. *Macromolecules* **2015**, *48*, 600−609.
(28) Lee, J.; Han, S.; Kim, M.; Kim, B.-S. Anionic Polymerization of Azidoalkyl Glycidyl Ethers and Post-Polymerization Modification. *Macromolecules* **2020**, *53*, 355−366.
(29) Hwang, E.; Kim, K.; Lee, C. G.; Kwon, T.-H.; Lee, S.-H.; Min, S. K.; Kim, B.-S. Tailorable Degradation of pH-Responsive All-Polyether Micelles: Unveiling the Role of Monomer Structure and Hydrophilic−Hydrophobic Balance. *Macromolecules* **2019**, *52*, 5884−5893.
(30) Verkoyen, P.; Frey, H. Long-Chain Alkyl Epoxides and Glycidyl Ethers: An Underrated Class of Monomers. *Macromol. Rapid Commun.* **2020**, *41*, 2000225.
(31) Linker, O.; Blankenburg, J.; Maciol, K.; Bros, M.; Frey, H. Ester Functional Epoxide Monomers for Random and Gradient Poly(ethylene glycol) Polyelectrolytes with Multiple Carboxylic Acid Moieties. *Macromolecules* **2020**, *53*, 3524−3534.
(32) Murakami, T.; Kawamori, T.; Gopez, J. D.; McGrath, A. J.; Klinger, D.; Saito, K. Synthesis of PEO-Based Physical Gels with Tunable Viscoelastic Properties. *J. Polym. Sci., Part A: Polym. Chem.* **2018**, *56*, 1033−1038.
(33) Jung, P.; Ziegler, A. D.; Blankenburg, J.; Frey, H. Glycidyl Tosylate: Polymerization of a "Non-Polymerizable" Monomer Permits Universal Post-Functionalization of Polyethers. *Angew. Chem., Int. Ed.* **2019**, *58*, 12883−12886.
(34) Herzberger, J.; Fischer, K.; Leibig, D.; Bros, M.; Thiermann, R.; Frey, H. Oxidation-Responsive and "Clickable" Poly(ethylene glycol) via Copolymerization of 2-(Methylthio)ethyl Glycidyl Ether. *J. Am. Chem. Soc.* **2016**, *138*, 9212−9223.
(35) Sunder, A.; Türk, H.; Haag, R.; Frey, H. Copolymers of Glycidol and Glycidyl Ethers: Design of Branched Polyether Polyols by Combination of Latent Cyclic AB_2 and ABR Monomers. *Macromolecules* **2000**, *33*, 7682−7692.
(36) Obermeier, B.; Frey, H. Poly(ethylene glycol-co-allyl glycidyl ether)s: A PEG-Based Modular Synthetic Platform for Multiple Bioconjugation. *Bioconjugate Chem.* **2011**, *22*, 436−444.
(37) Blasco, E.; Sims, M. B.; Goldmann, A. S.; Sumerlin, B. S.; Barner-Kowollik, C. *50th Anniversary Perspective*: Polymer Functionalization. *Macromolecules* **2017**, *50*, 5215−5252.
(38) Lee, J.; McGrath, A. J.; Hawker, C. J.; Kim, B.-S. pH-Tunable Thermoresponsive PEO-Based Functional Polymers with Pendant Amine Groups. *ACS Macro Lett.* **2016**, *5*, 1391−1396.
(39) Lee, B. F.; Kade, M. J.; Chute, J. A.; Gupta, N.; Campos, L. M.; Fredrickson, G. H.; Kramer, E. J.; Lynd, N. A.; Hawker, C. J. Poly(allyl glycidyl ether)-A Versatile and Functional Polyether Platform. *J. Polym. Sci., Part A: Polym. Chem.* **2011**, *49*, 4498−4504.
(40) Kang, T.; Amir, R. J.; Khan, A.; Ohshimizu, K.; Hunt, J. N.; Sivanandan, K.; Montañez, M. I.; Malkoch, M.; Ueda, M.; Hawker, C. J. Facile Access to Internally Functionalized Dendrimers through Efficient and Orthogonal Click Reactions. *Chem. Comm.* **2010**, *46*, 1556−1558.
(41) Fellin, C. R.; Adelmund, S. M.; Karis, D. G.; Shafranek, R. T.; Ono, R. J.; Martin, C. G.; Johnston, T. G.; DeForest, C. A.; Nelson, A. Tunable Temperature- and Shear-Responsive Hydrogels Based on Poly(alkyl glycidyl ether)s. *Polym. Int.* **2019**, *68*, 1238−1246.
(42) Zhang, M.; Vora, A.; Han, W.; Wojtecki, R. J.; Maune, H.; Le, A. B. A.; Thompson, L. E.; McClelland, G. M.; Ribet, F.; Engler, A. C.; Nelson, A. Dual-Responsive Hydrogels for Direct-Write 3D Printing. *Macromolecules* **2015**, *48*, 6482−6488.
(43) Sayuri, A.; Aya, K.; Shin-ichiro, I.; Masayoshi, W. Novel Thermosensitive Polyethers Prepared by Anionic Ring-Opening Polymerization of Glycidyl Ether Derivatives. *Chem. Lett.* **2002**, *31*, 1128−1129.
(44) Ogura, M.; Tokuda, H.; Imabayashi, S.-i.; Watanabe, M. Preparation and Solution Behavior of a Thermoresponsive Diblock Copolymer of Poly(ethyl glycidyl ether) and Poly(ethylene oxide). *Langmuir* **2007**, *23*, 9429−9434.
(45) Isono, T.; Miyachi, K.; Satoh, Y.; Sato, S.-i.; Kakuchi, T.; Satoh, T. Design and Synthesis of Thermoresponsive Aliphatic Polyethers with a Tunable Phase Transition Temperature. *Polym. Chem.* **2017**, *8*, 5698−5707.
(46) Tsuda, R.; Kaino, S.; Kokubo, H.; Imabayashi, S.-I.; Watanabe, M. Effect of Core-Shell Micelle Formation on the Redox Properties of Phenothiazine-Labeled Poly(ethyl glycidy ether)-*Block*-Poly(ethylene oxide). *Colloids Surf., B* **2007**, *56*, 255−259.
(47) Zhang, X.; Waymouth, R. M. 1,2-Dithiolane-Derived Dynamic, Covalent Materials: Cooperative Self-Assembly and Reversible Cross-Linking. *J. Am. Chem. Soc.* **2017**, *139*, 3822−3833.

https://dx.doi.org/10.1021/acs.biomac.0c01140
Biomacromolecules XXXX, XXX, XXX−XXX

(48) Meng, F.; Hennink, W. E.; Zhong, Z. Reduction-Sensitive Polymers and Bioconjugates for Biomedical Applications. *Biomaterials* **2009**, *30*, 2180−2198.
(49) Peters, A. J.; Lodge, T. P. Comparison of Gel Relaxation Times and End-Block Pullout Times in ABA Triblock Copolymer Networks. *Macromolecules* **2016**, *49*, 7340−7349.
(50) Tsitsilianis, C.; Serras, G.; Ko, C.-H.; Jung, F.; Papadakis, C. M.; Rikkou-Kalourkoti, M.; Patrickios, C. S.; Schweins, R.; Chassenieux, C. Thermoresponsive Hydrogels Based on Telechelic Polyelectrolytes: From Dynamic to "Frozen" Networks. *Macromolecules* **2018**, *51*, 2169−2179.
(51) Zinn, T.; Willner, L.; Lund, R. Telechelic Polymer Hydrogels: Relation between the Microscopic Dynamics and Macroscopic Viscoelastic Response. *ACS Macro Lett.* **2016**, *5*, 1353−1356.
(52) Trudel, J.; Massia, S. P. Assessment of the Cytotoxicity of Photocrosslinked Dextran and Hyaluronan-Based Hydrogels to Vascular Smooth Muscle Cells. *Biomaterials* **2002**, *23*, 3299−3307.
(53) Park, K.; Dawson, J. I.; Oreffo, R. O. C.; Kim, Y.-H.; Hong, J. Nanoclay−Polyamine Composite Hydrogel for Topical Delivery of Nitric Oxide Gas via Innate Gelation Characteristics of Laponite. *Biomacromolecules* **2020**, *21*, 2096−2103.

https://dx.doi.org/10.1021/acs.biomac.0c01140
Biomacromolecules XXXX, XXX, XXX−XXX